IEEE Access
Multidisciplinary | Rapid Review | Open Access Journal

Received 1 December 2022, accepted 17 December 2022, date of publication 20 December 2022,
date of current version 27 December 2022.

Digital Object Identifier 10.1109/ACCESS.2022.3230967

RESEARCH ARTICLE

Passivity-Based Robust Controller Design for Load-Independent Voltage Source Inverters

KENTA KOIWA, (Member, IEEE), TAIKI GOTO, TADANAO ZANMA, (Member, IEEE), AND KANG-ZHI LIU, (Senior Member, IEEE)
Department of Electrical and Electronic Engineering, Chiba University, Chiba 263-8522, Japan
Corresponding author: Kenta Koiwa (kenta.koiwa@chiba-u.jp)

This work was supported by JSPS KAKENHI under Grant JP22K14233.

ABSTRACT We propose a novel voltage controller design procedure for voltage source inverters (VSIs) with uncertain loads, focusing on the passivity of loads. VSIs have been widely used in many applications. A VSI must regulate the load voltage to its sinusoidal reference quickly and accurately without distortion. It is essential to design a voltage controller that takes into account various load conditions since it is rarely known in advance what types of loads are connected to the VSI. In particular, it is challenging to suppress the voltage harmonic distortion caused by a nonlinear load, such as a diode rectifier, while achieving fast-tracking and zero steady-state error. A controller designed by the proposed procedure guarantees robust stability of the VSI independent of the load type and value. Namely, no information about uncertainties of load is needed to stabilize the VSI. Moreover, the proposed procedure realizes zero-steady state error, fast-tracking, and low distortion. We demonstrate the effectiveness of the proposed controller through comparative analysis with the proportional resonant (PR) and conventional robust controllers via simulations and experiments.

INDEX TERMS Robust control, voltage source inverter, positive realness, linear matrix inequality.

I. INTRODUCTION

Voltage source inverters (VSIs), which convert DC voltage into AC voltage, have been widely used in many applications such as industrial equipment, uninterruptible power supplies (UPSs), and distributed generators [1], [2], [3], [4], [5], [6], [7], [8]. In stand-alone applications, such as UPSs, the VSI must regulate the load voltage to its sinusoidal reference quickly and accurately without distortion [2], [7], [9], [10], [11], [12], [13], [14], [15]. It is not an easy task to design a voltage controller for VSIs due to the uncertain load and the resonance of the LC filter connected to the VSI [3], [16], [17], [18]. In particular, it is essential to design a voltage controller that takes into account various load conditions since it is rarely known in advance what types of loads are connected to the VSI.

Numerous studies have been developed for the VSI voltage controller that can achieve zero steady-state error, fast-tracking, and low distortion while stabilizing the VSI. Combining the proportional-integral controller and the dq transformation achieves zero steady-state error [11], [14], [19], [20]. Nevertheless, additional mechanisms are required in the dq transformation for a single-phase VSI [11], [20]. Moreover, cross-couplings on the dq-frame degrade control performance in the system, and an additional current sensor is needed to independently control the dq-voltage (current) [19]. Proportional resonant (PR) controllers on the stationary frame has been widely used for the voltage control of the VSI due to their simple structure [3], [4], [7], [14], [21]. The PR controller regulates the load voltage to its sinusoidal reference with no steady-state error. However, it is difficult to achieve high-speed and accurate tracking with low distortion. In addition, the PR controller does not guarantee stability and performance of the VSI for uncertain loads. A dead-beat control for the VSI was proposed in [1] and [22]. The dead-beat control achieves a fast and accurate voltage response for VSIs with a known load, but the performance degrades when the load varies. Other VSI voltage controllers were proposed

The associate editor coordinating the review of this manuscript and approving it for publication was Engang Tian.

based on sliding mode control (SMC) [5], [9], [10], with some advantages such as fast response and robustness against parameters. However, these controllers based on the SMC have disadvantages, such as variable switching frequency, steady-state error, and chattering [12]. Furthermore, an additional current sensor is needed. For the stability of VSIs with uncertain loads, Lyapunov-function-based controllers were proposed in [12] and [15]. Although these controllers stabilize the VSI irrespective of load type, it is still challenging to consider control performance, such as fast-tracking and low distortion in the design.

Robust control is one promising method that addresses uncertainties in systems [23]. Some approaches based on robust control theories have been reported for VSIs [16], [17], [18], [24]. In [24], the linear quadratic regulator and backstepping method were presented to design a robust optimal state-feedback controller. This controller stabilizes VSIs with uncertain linear loads based on the small gain theorem. However, the stability and performance of VSIs with nonlinear loads have not been investigated. In addition, this method cannot handle specifications in the frequency domain. Robust control based on $\mathcal{H}_\infty$ control theory enables us to analyze specifications in the frequency domain, guaranteeing the robust stability and the performance of VSIs with uncertain linear loads [16], [17], [18]. In [16], a state feedback controller was designed based on $\mathcal{H}_\infty$ control theory. However, an additional current sensor was required, and the suppression of distortion due to a nonlinear load was not investigated. Output-feedback controllers for VSIs based on $\mathcal{H}_\infty$ control theory were proposed in [16] and [18]. The controllers guarantee robust stability and performance of VSIs with uncertain linear loads without a current sensor. Furthermore, the controller proposed in [18] can reduce voltage harmonic distortion caused by the diode rectifier load while achieving fast-tracking and zero steady-state error. Nevertheless, load types are limited to inductance and resistance loads with known minimum values. The stability for nonlinear loads, such as the diode rectifier is not guaranteed.

In this paper, we propose a novel voltage controller design procedure for VSIs with uncertain loads by focusing on the passivity of loads [25]. This problem setting is not limited since loads connected to the VSI are generally passive in stand-alone applications. A controller designed by the proposed procedure guarantees robust stability of the VSI regardless of load type and uncertainty if they satisfy passivity. In addition, no information about uncertainties of the load is needed to stabilize the VSI, nor is an additional current sensor due to the output feedback. Moreover, our proposed procedure can satisfy zero steady-state error, fast-tracking, and low distortion, which are considered through the weighting functions in the frequency domain design. We demonstrate the effectiveness of the proposed controller through comparative analysis with the PR and conventional robust controllers via simulations and experiments.

The rest of this paper is organized as follows: Section II describes the preliminary mathematical notations, system configuration, and robust control theory that form the basis of the proposed controller synthesis. In Section III, we propose a novel robust controller design method for VSIs with passive but uncertain loads. Simulations and experiments are demonstrated in Section IV to show the effectiveness of the proposed controller. Section V concludes this paper.

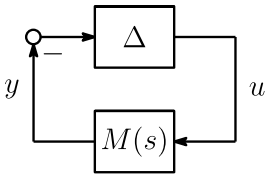

FIGURE 1. Closed-loop system.

II. PRELIMINARIES

Notation: $\mathbb{R}^n$ and $\mathbb{R}^{m\times n}$ denote the set of n-dimensional real vectors and the set of $m \times n$ real matrices, respectively. $\mathbb{S}^n_{++}$ stands for the set of real positive definite matrix of size n, respectively. For a matrix $V \in \mathbb{R}^{n\times n}$, $V > 0$ ($V < 0$) denotes a positive (negative) definite matrix. I_n is the identity matrix of size n. For convenience, n_x denotes the dimension of x, i.e., $x \in \mathbb{R}^{n_x}$. $\mathrm{He}(X) := X + X^\intercal$. (A, B, C, D) denotes $D + C(sI - A)^{-1}B$.

For a transfer function $G(s)$, its $\mathcal{H}_\infty$-norm is denoted as $\|G\|_\infty$. The conjugate transpose of $G(\mathrm{j}\omega)$ is represented by $G^*(\mathrm{j}\omega) := G^\intercal(-\mathrm{j}\omega)$. The real and imaginary parts of $G(\mathrm{j}\omega)$ are denoted as $\mathrm{Re}(G(\mathrm{j}\omega))$ and $\mathrm{Im}(G(\mathrm{j}\omega))$, respectively. For simplicity, the time function and its Laplace transform are given by the same notation, such as $x(t)$ and $x(s)$. A signal $x(t)$ is abbreviated as x whenever it is clear from the context.

Definition 1: [23] A stable transfer matrix $M(s)$ is called positive-real if

$$M^*(\mathrm{j}\omega) + M(\mathrm{j}\omega) \geq 0 \quad \forall\omega \in [-\infty, \infty]. \tag{1}$$

Specifically, $M(s)$ is called strongly positive-real when

$$M^*(\mathrm{j}\omega) + M(\mathrm{j}\omega) > 0 \quad \forall\omega \in [-\infty, \infty]. \tag{2}$$

In single-input and single-output systems, if $M(s)$ is strongly positive-real, $\mathrm{Re}(M(\mathrm{j}\omega))$ is non-negative. Therefore, if $M(s)$ is positive-real (strongly positive-real), the Nyquist diagram of $M(s)$ is in the (open) right half plane and the phase angle is limited to $[-90°, 90°]$ $((-90°, 90°))$.

Theorem 1: In the closed-loop system shown in Fig. 1, assume that uncertainty Δ is stable and positive-real. Then, the closed-loop system is asymptotically stable if $M(s)$ is stable and strongly positive-real [23], [26].

Proof: See [23].

A. VSI

Fig. 2 shows the system configuration addressed in this paper. The single-phase VSI is connected to the load through the LC filter. Table 1 lists the notations used in this paper. When the harmonics caused by the pulse width modulation (PWM) and dynamics of the VSI are ignored, v_i can be regarded as

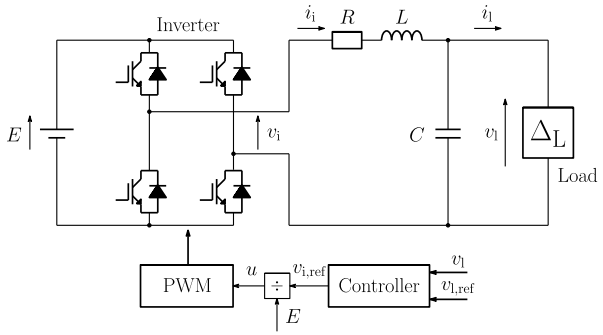

FIGURE 2. System configuration.

TABLE 1. Notations.

v	voltage
i	current
$\bar{v}$	effective value of v
S_n	rated capacity of the VSI
$u\ (-1 \le u \le 1)$	modulation signal
E	DC link voltage
L	inductance
R	internal resistance in inductor L
C	capacitance
ω	angular frequency
(subscript)	for state/signal x
x_i	x on VSI side
x_l	x on load side
x_n	rated value of x
x_ref	reference of x

$v_\mathrm{i} \approx Eu = v_\mathrm{i,ref}$. In this paper, we investigate not only linear loads such as resisters, inductors, and capacitors, but also non-linear loads composed of diode rectifiers. The load is denoted as $\Delta_\mathrm{L} = v_\mathrm{l}/i_\mathrm{l}$. From Fig. 2, the transfer function $G_{v_\mathrm{l}v_\mathrm{i}}(s)$ from v_i to v_l is given by

$$G_{v_\mathrm{l}v_\mathrm{i}}(s) = \frac{v_\mathrm{l}(s)}{v_\mathrm{i}(s)} = \frac{1}{LCs^2 + (RC + \frac{L}{\Delta_\mathrm{L}})s + \frac{R}{\Delta_\mathrm{L}} + 1}. \quad (3)$$

The controller should be designed to satisfy the following specifications regardless of loads:
The load voltage v_l

- S-1) is regulated to the sinusoidal reference $v_\mathrm{l,ref}$ with no steady-state error,
- S-2) has low distortion, and
- S-3) is unaffected by the sensor noise in high frequency regions.

We emphasize that our method can be extended to three-phase inverters since they can be regarded as two independent circuits through Clarke's transformation.

B. ROBUST CONTROLLER SYNTHESIS FOR SYSTEMS WITH POSITIVE-REAL UNCERTAINTY

We briefly review the method proposed in [25], which is the basis of the proposed controller design described in the next section.

Fig. 3 shows an output feedback control system. In Fig. 3, Δ_pr represents uncertainty and is assumed to be positive-real,

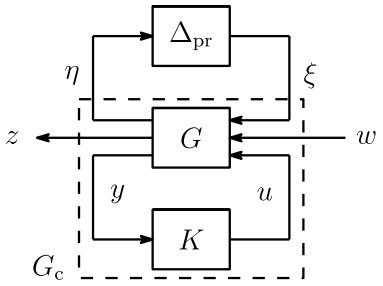

FIGURE 3. Output feedback control system with positive-real uncertainty.

G is a generalized plant composed of nominal plant and weighting functions for performance specifications, K is a controller, and G_c is the nominal closed-loop system composed of G and K. In addition, u and y are the input and output of G, η and ξ are the input and output of Δ_pr, and w is disturbance and z is performance output.

For the system shown in Fig. 3, its robust performance index is

$$\|H_{zw}\|_\infty < 1, \quad (4)$$

where $H_{zw}(s)$ is the transfer function from w to z.

In Fig. 3, G and K are given as follows:

$$G : \begin{bmatrix} \dot{x} \\ \eta \\ z \\ y \end{bmatrix} = \begin{bmatrix} A & B_1 & B_2 & B_3 \\ C_1 & D_{11} & D_{12} & D_{13} \\ C_2 & D_{21} & D_{22} & D_{23} \\ C_3 & D_{31} & D_{32} & 0 \end{bmatrix} \begin{bmatrix} x \\ \xi \\ w \\ u \end{bmatrix}, \quad (5)$$

and

$$K : \begin{bmatrix} \dot{x}_K \\ u \end{bmatrix} = \begin{bmatrix} A_K & B_K \\ C_K & D_K \end{bmatrix} \begin{bmatrix} x_K \\ y \end{bmatrix}. \quad (6)$$

In (5) and (6), x and x_K denote the states of G and K, respectively. From (5) and (6), G_c is as follows:

$$G_\mathrm{c} : \begin{bmatrix} \dot{x}_c \\ \eta \\ z \end{bmatrix} = \begin{bmatrix} \mathcal{A}_c & \mathcal{B}_{c1} & \mathcal{B}_{c2} \\ \mathcal{C}_{c1} & \mathcal{D}_{c11} & \mathcal{D}_{c12} \\ \mathcal{C}_{c2} & \mathcal{D}_{c21} & \mathcal{D}_{c22} \end{bmatrix} \begin{bmatrix} x_c \\ \xi \\ w \end{bmatrix}, \quad (7)$$

where $x_c = \begin{bmatrix} x^\intercal & x_K^\intercal \end{bmatrix}^\intercal$,

$$\mathcal{A}_c = \begin{bmatrix} A + B_3 D_K C_3 & B_3 C_K \\ B_K C_3 & A_K \end{bmatrix}, \quad (8)$$

$$\mathcal{B}_{cj} = \begin{bmatrix} B_j + B_3 D_K D_{3j} \\ B_K D_{3j} \end{bmatrix}, \quad (9)$$

$$\mathcal{C}_{ci} = \begin{bmatrix} C_i + D_{i3} D_K C_3 & D_{i3} C_K \end{bmatrix}, \quad (10)$$

$$\mathcal{D}_{cij} = D_{ij} + D_{i3} D_K D_{3j}, \quad (11)$$

for $i = 1, 2$ and $j = 1, 2$ [23].

For the subsequent discussion, we define

$$\mathcal{P} = \Pi_2 \Pi_1^{-1}, \quad \mathcal{P}\Pi_1 = \Pi_2,$$
$$\Pi_1 := \begin{bmatrix} X & I_{n_x} \\ M^\intercal & 0 \end{bmatrix}, \quad \Pi_2 := \begin{bmatrix} I_{n_x} & Y \\ 0 & N^\intercal \end{bmatrix},$$

where $XY + MN^\intercal = I_{n_x}$, $X \in \mathbb{S}^{n_x}_{++}$, $Y \in \mathbb{S}^{n_x}_{++}$, $M \in \mathbb{R}^{n_x \times n_x}$, $N \in \mathbb{R}^{n_x \times n_x}$, and

$$A^\dagger := NA_K M^\intercal + NB_K C_3 X + YB_3 C_K M^\intercal + Y(A + B_3 D_K C_3)X \in \mathbb{R}^{n_x \times n_x}, \quad (12)$$

$$B^\dagger := NB_K + YB_3 D_K \in \mathbb{R}^{n_x \times n_y}, \quad (13)$$

$$C^\dagger := C_K M^\intercal + D_K C_3 X \in \mathbb{R}^{n_u \times n_x}, \quad (14)$$

$$D^\dagger := D_K \in \mathbb{R}^{n_u \times n_y}. \quad (15)$$

For the system shown in Fig. 3, the following theorem is known [25]:

Theorem 2: For all positive-real uncertainties, there exists a controller which guarantees the closed-loop stability and the robust performance specified by (4) if there exist $A^\dagger$, $B^\dagger$, $C^\dagger$, $D^\dagger$, X, Y, and a constant $\lambda > 0$ satisfying

$$\mathrm{He}\begin{bmatrix} \Pi_1^\intercal \mathcal{P}\mathcal{A}_c\Pi_1 & \Pi_1^\intercal \mathcal{P}\mathcal{B}_{c1} & \Pi_1^\intercal \mathcal{P}\mathcal{B}_{c2} & \Pi_1^\intercal C_{c2}^\intercal \\ \mathcal{C}_{c1}\Pi_1 & \mathcal{D}_{c11} & \mathcal{D}_{c12} & \mathcal{D}_{c21}^\intercal \\ 0 & 0 & -\frac{1}{2\lambda} I_{n_w} & \mathcal{D}_{c22}^\intercal \\ 0 & 0 & 0 & -\frac{\lambda}{2} I_{n_z} \end{bmatrix} < 0, \quad (16)$$

$$\begin{bmatrix} X & I_{n_x} \\ I_{n_x} & Y \end{bmatrix} > 0, \quad (17)$$

where

$$\Pi_1^\intercal \mathcal{P}\Pi_1 = \Pi_2^\intercal \Pi_1 = \begin{bmatrix} X & I_{n_x} \\ I_{n_x} & Y \end{bmatrix}, \quad (18)$$

$$\Pi_1^\intercal \mathcal{P}\mathcal{A}_c\Pi_1 = \begin{bmatrix} AX + B_3 C^\dagger & A + B_3 D^\dagger C_3 \\ A^\dagger & YA + B^\dagger C_3 \end{bmatrix}, \quad (19)$$

$$\Pi_1^\intercal \mathcal{P}\mathcal{B}_{cj} = \begin{bmatrix} B_j + B_3 D^\dagger D_{3j} \\ YB_j + B^\dagger D_{3j} \end{bmatrix}, \quad (20)$$

$$\mathcal{C}_{ci}\Pi_1 = \begin{bmatrix} C_i X + D_{i3} C^\dagger & C_i + D_{i3} D^\dagger C_3 \end{bmatrix}, \quad (21)$$

for $i = 1, 2$ and $j = 1, 2$.

Proof: See [25].

If (16) and (17) are solvable, there exist nonsingular M and N satisfying $I_{n_x} - XY = MN^\intercal$. Thus, we obtain each matrix in (6) as follows:

$$D_K = D^\dagger, \quad (22)$$

$$C_K = (C^\dagger - D_K C_3 X)(M^{-1})^\intercal, \quad (23)$$

$$B_K = N^{-}1(B^\dagger - YB_3 D_K), \quad (24)$$

$$A_K = N^{-1}(A^\dagger - NB_K C_3 X - YB_3 C_K M^\intercal - Y(A + B_3 D_K C_3)X)(M^{-1})^\intercal. \quad (25)$$

Let $H_{\eta\xi}(s)$ be the transfer function from ξ to η, then $-H_{\eta\xi}(s)$ is strongly positive-real [25]. Therefore, from Theorem 1, the closed-loop system of $H_{\eta\xi}(s)$ and Δ_{pr} shown in Fig. 3 is asymptotically stable.

III. PROPOSED ROBUST CONTROLLER DESIGN PROCEDURE FOR VSI

This section proposes a novel voltage controller design procedure for VSIs based on Theorem 2. The proposed controller ensures robust stability and high performance in VSIs regardless of linear or nonlinear load.

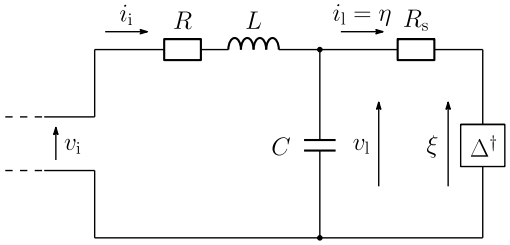

FIGURE 4. Equivalent circuit.

A. PRE-PROCESSING

The controller is designed based on Theorem 2. Unfortunately, Theorem 2 cannot be applied directly when

- P-1) $\Delta_{\mathrm{L}} = 0$, which implies the short-circuit shown in Fig. 2, and/or
- P-2) $G_{v_{\mathrm{l}}v_{\mathrm{i}}}(s)$ in (3) includes two loads, Δ_{L}.

We introduce some techniques to avoid P-1) and P-2). First, to avoid P-1), let Δ_{L} be partitioned as

$$\Delta_{\mathrm{L}} := \Delta^\dagger + R_{\mathrm{s}}, \quad (26)$$

where $\Delta^\dagger$ is passive and $R_{\mathrm{s}} > 0$ is small. From (26), the equivalent circuit shown in Fig. 2 can be redrawn as Fig. 4. The circuit shown in Fig. 4 includes no short circuit even when $\Delta^\dagger = 0$ due to R_{s}. Therefore, we can avoid P-1) by only regarding $\Delta^\dagger$ as uncertainty. Namely, the robust stability and performance in the VSI are guaranteed for Δ_{L} satisfying $R_{\mathrm{s}} \le \mathrm{Re}(\Delta_{\mathrm{L}}(\mathrm{j}\omega))$.[1] Note that the load region which ensures robust stability and performance becomes small when R_{s} is large. Specifically, when $R_{\mathrm{s}} > \frac{(\bar{v}_{\mathrm{l,n}})^2}{S_{\mathrm{n}}}$ where $\frac{(\bar{v}_{\mathrm{l,n}})^2}{S_{\mathrm{n}}}$ is the rated load, robust stability and performance are not guaranteed at the rated load. This implies that (26) is not satisfied when $R_{\mathrm{s}} > \mathrm{Re}(\Delta_{\mathrm{L}}(\mathrm{j}\omega))$ since $\Delta^\dagger$ is not passive. Therefore, R_{s} is determined such that

$$0 < R_{\mathrm{s}} \le \frac{(\bar{v}_{\mathrm{l,n}})^2}{S_{\mathrm{n}}}. \quad (27)$$

Note that R_{s} is not the actual resistor but a virtual one for the controller design. Moreover, it is not necessary to know the variation range of loads in advance, unlike standard robust control approaches [23].

Next, we give a solution to P-2). We recast (3), substituting (26) into it as follows:

$$G_{v_{\mathrm{l}}v_{\mathrm{i}}}(s) = \frac{1}{LCs^2 + (RC + \frac{L}{\Delta^\dagger + R_{\mathrm{s}}})s + \frac{R}{\Delta^\dagger + R_{\mathrm{s}}} + 1} = \frac{1}{Ls + R} \cdot \frac{G_1(s)}{1 + G_1(s)\frac{R_{\mathrm{s}}^{-1}}{1 + R_{\mathrm{s}}^{-1}\Delta^\dagger}}, \quad (28)$$

where

$$G_1(s) = \frac{Ls + R}{LCs^2 + RCs + 1}. \quad (29)$$

[1] In practice, passive loads composed of resistors, inductors, and capacitors satisfy these characteristics.

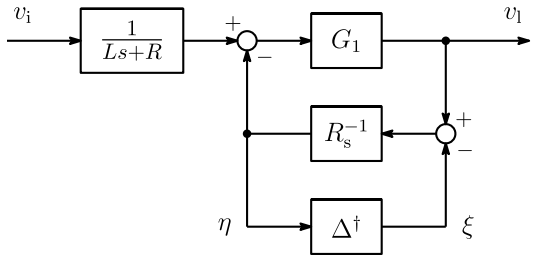

FIGURE 5. Block diagram from v_i to v_l.

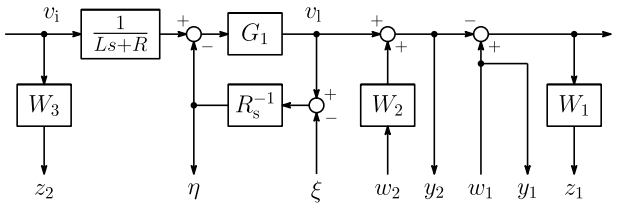

FIGURE 6. Generalized plant in the proposed method.

From (28), we obtain the block diagram shown in Fig. 5. We can set a generalized plant of the system shown in Fig. 6, Thus, we can design a controller of the VSI by Theorem 2. It is emphasized Theorem 2 guarantees that the proposed controller achieves robust stability and performance in the VSI with any passive loads. Specifically, no information about the unknown loads other than passivity is needed in advance to stabilize the VSI.

B. PROPOSED DESIGN PROCEDURE

We provide the following design procedure of the VSI controller for given parameters S_n, $\bar{v}_{\mathrm{l,n}}$, L, and C of the system shown in Fig. 2:

D-1) Set R_s to satisfy (27).
D-2) Obtain $G_{v_\mathrm{l}v_\mathrm{i}}(s)$ in (28).
D-3) Set the generalized plant as shown in Fig. 6.
D-4) Set $W_1(s)$, $W_2(s)$, and $W_3(s)$ to meet S-1)–S-3).
D-5) Obtain the controller from (22)–(25) by solving (16) and (17).

In Fig. 6, $w_1(=v_{\mathrm{l,ref}})$ is the reference, w_2 is the sensor noise, z_1 is the performance output to evaluate the tracking of v_l to $v_{\mathrm{l,ref}}$, z_2 is the performance output to evaluate the controller output, and y_1 and y_2 are the reference signal and load voltage measured by the voltage sensor, respectively.

In D-3), we utilize $v_{\mathrm{l,ref}}$ in the controller to achieve fast tracking, i.e., to use a two-degrees of freedom output-feedback controller:

$$v_{\mathrm{i,ref}}(s) = \underbrace{\begin{bmatrix} K_{\mathrm{FF}}(s) & K_{\mathrm{FB}}(s) \end{bmatrix}}_{K} \begin{bmatrix} v_{\mathrm{l,ref}}(s) \\ v_\mathrm{l}(s) \end{bmatrix}. \tag{30}$$

In D-4), $W_1(s)$, $W_2(s)$, and $W_3(s)$ are tuned such that

W-1) $W_1(s)$ is a low-pass filter with resonances at $i\omega_{\mathrm{ref}}$, $i = (1, 3, 5\ldots)$ for S-1) and S-2), and
W-2) $W_2(s)$ and $W_3(s)$ are high pass filters for S-3).

TABLE 2. Parameters of VSI.

S_n	1 kVA	$\bar{v}_{\mathrm{l,n}}$	220 V
ω_{ref}	$2\pi \cdot 50$ rad/s	L	3.07 mH
R	43.2 mΩ	C	47 μF

Zero steady-state error and low distortion in v_l can be achieved since the resultant controller has resonances at $i\omega_{\mathrm{ref}}$, $(i = 1, 3, 5, \ldots)$ due to W-1). Specifically, the distortion caused by the diode rectifier load can be significantly suppressed by the resonances [11]. In addition, the resultant controller has low gain in the high frequency region due to W-1). This implies that a VSI with the controller is not sensitive to sensor noise.

C. DESIGN EXAMPLE

We design a controller for the parameters listed in Table 2 with the proposed design procedure D-1)–D-5).

In D-1), set $R_\mathrm{s} = 1\ \Omega$ to satisfy (27).
In D-2), obtain $G_{v_\mathrm{l}v_\mathrm{i}}(s)$ from (28).
In D-3), set the generalized plant shown in Fig. 6.
In D-4), set

$$W_1(s) = \frac{1 \cdot 10^5}{s^2 + 0.002s + \omega_{\mathrm{ref}}^2} \cdot \prod_{i=3,5,\ldots,13} \frac{s^2 + 100s + (i\omega_{\mathrm{ref}})^2}{s^2 + 0.002s + (i\omega_{\mathrm{ref}})^2}, \tag{31}$$

$$W_2(s) = W_3(s) = 0.08 \left(\frac{\omega_2^2(s^2 + 2\zeta\omega_1 s + \omega_1^2)}{\omega_1^2(s^2 + 2\zeta\omega_2 s + \omega_2^2)} \right)^2, \tag{32}$$

where $\zeta = 0.5$, $\omega_1 = 2\pi \cdot 4 \cdot 10^3$, and $\omega_2 = 2\pi \cdot 13 \cdot 10^3$.

In D-5), obtain the controller from (22)–(25) by solving (16) and (17) with $\lambda = 1$ using Robust Control Toolbox in MATLAB.

Fig. 7 shows the Bode plots of (31) and (32). Note that we consider harmonic suppression up to the 13th order in (31).

Fig. 8 shows the Bode plot of the resultant controller. As shown in Fig. 8, the controller has a wide bandwidth, resonances at $i\omega_{\mathrm{ref}}$, $(i = 1, 3, \ldots, 13)$, and low gain in the high frequency region. Therefore, the controller designed via the proposed procedure can achieve fast tracking and low distortion.

IV. SIMULATIONS AND EXPERIMENTS

We validate the effectiveness of the proposed method by comparing it with a conventional robust controller [18] (hereafter denoted as μ-controller; see Appendix A for μ-controller) and a standard PR controller through simulations and experiments. In the simulations, we investigate the effectiveness of the proposed controller in a large-scale model; the rated capacity of the VSI is 1 kVA. In the experiments, we use a scaled-down model; the rated capacity of the VSI is 51.7 VA. We consider both an RL load (linear load) and a diode rectifier load (nonlinear load) shown in Fig. 9 [27]. Table 3 lists the system parameters. In the simulations, R_{dl} and C_d as

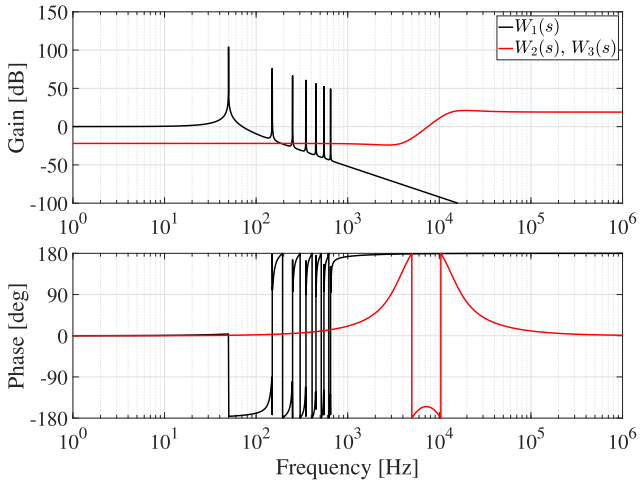

FIGURE 7. Weights in the proposed method.

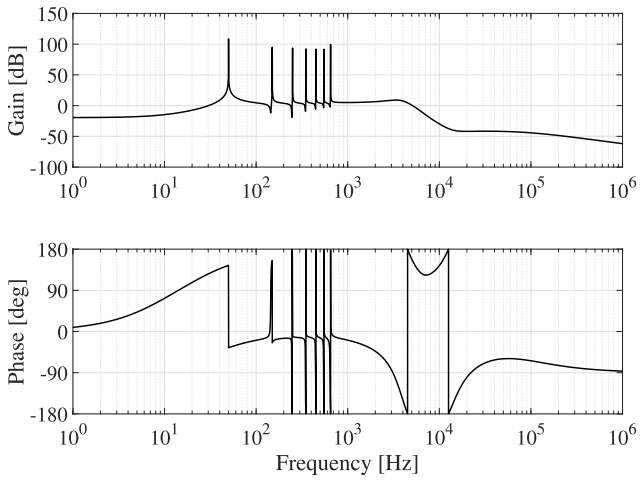

(a) $K_{\mathrm{FF}}(s)$.

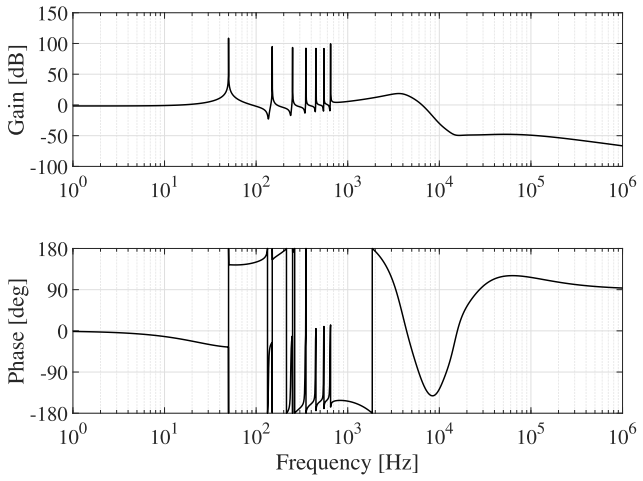

(b) $K_{\mathrm{FB}}(s)$.

FIGURE 8. Bode plots of the proposed controller.

determined by [27] are used. In the experiments, available R_{d1} and C_{d} are used in our laboratory. Note that the LC filter

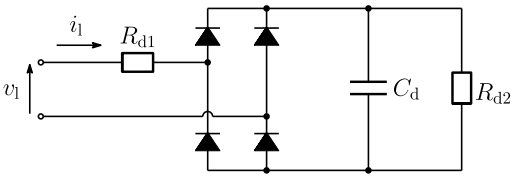

FIGURE 9. Diode rectifier load.

TABLE 3. Parameters for simulations and experiments.

Simulation	
S_{n}	1 kVA
$\bar{v}_{\mathrm{l,n}}$	220 V
E	400 V
Diode rectifier load	$R_{\mathrm{d1}} = 1.94\ \Omega$, $R_{\mathrm{d2}} = 72.0\ \Omega$, $C_{\mathrm{d}} = 1374\ \mu$F
Experiment	
S_{n}	51.7 VA
$\bar{v}_{\mathrm{l,n}}$	50 V
E	100 V
Diode rectifier load	$R_{\mathrm{d1}} = 2.1\ \Omega$, $R_{\mathrm{d2}} = 72.0\ \Omega$, $C_{\mathrm{d}} = 2000\ \mu$F
Simulation and experiment	
RL Load $\Delta_{\mathrm{L}} = R_{\mathrm{L}} + sL_{\mathrm{L}}$	$R_{\mathrm{L}} = 48.3\ \Omega$ and $L_{\mathrm{L}} = 10$ mH
ω_{ref}	$2\pi \cdot 50$ rad/s
Switching frequency	10 kHz
Sampling period (control period)	50 μs

parameters listed in Table 2 are used for the simulations and experiments.

We analyze the VSI with the proposed controller in terms of the $\mathcal{L}_{2\mathrm{e}}$-norm defied by

$$\left\| \frac{v_{\mathrm{l,ref}} - v_{\mathrm{l}}}{\bar{v}_{\mathrm{l,n}}} \right\|_{\mathcal{L}_{2\mathrm{e}}} := \left(\int_0^{\tau} \left(\frac{v_{\mathrm{l,ref}} - v_{\mathrm{l}}}{\bar{v}_{\mathrm{l,n}}} \right)^2 \mathrm{d}t \right)^{\frac{1}{2}}, \quad (33)$$

total harmonic distortion (THD), and robustness to load variations. Time responses for a sinusoidal voltage reference are investigated to evaluate these criteria in the simulations and experiments.

A. SIMULATIONS

We analyze the time responses for the sinusoidal voltage reference in which the amplitude of $v_{\mathrm{l,ref}}$ is changed from 0 to $\bar{v}_{\mathrm{l,n}}$ at 0 s. In this scenario, the values of R_{L} and R_{d2} are changed to twice the nominal values at 0.125 s, respectively. We performed this simulation using MATLAB/Simulink 2017b. In the simulation, the max step size is 10^{-7} in the variable-step mode.

Figs. 10 and 11 show the time responses of the load voltage. It can be observed from these figures that the voltage responses are faster in the proposed controller than the others. In addition, no overshoot or steady-state error occurs in the voltage response in the proposed controller. The proposed controller can stabilize the VSI regardless of linear and nonlinear load variations. By contrast, the time response by the PR controller is distorted when the load varies and diverges when the load is removed ($R = \infty$).

Table 4 lists the $\mathcal{L}_{2\mathrm{e}}$-norm ($\tau = 0.06$ s) and THD. In Table 4, the $\mathcal{L}_{2\mathrm{e}}$-norm by the proposed controller is less

TABLE 4. Performance indices (simulation).

	Proposed	μ	PR
$\mathcal{L}_{2e}$-norm (linear load)	0.0113	0.0215	0.0618
$\mathcal{L}_{2e}$-norm (nonlinear load)	0.0283	0.0386	0.0745
THD (linear load) [%]	0.03	0.03	0.00
THD (nonlinear load) [%]	0.95	1.25	17.18

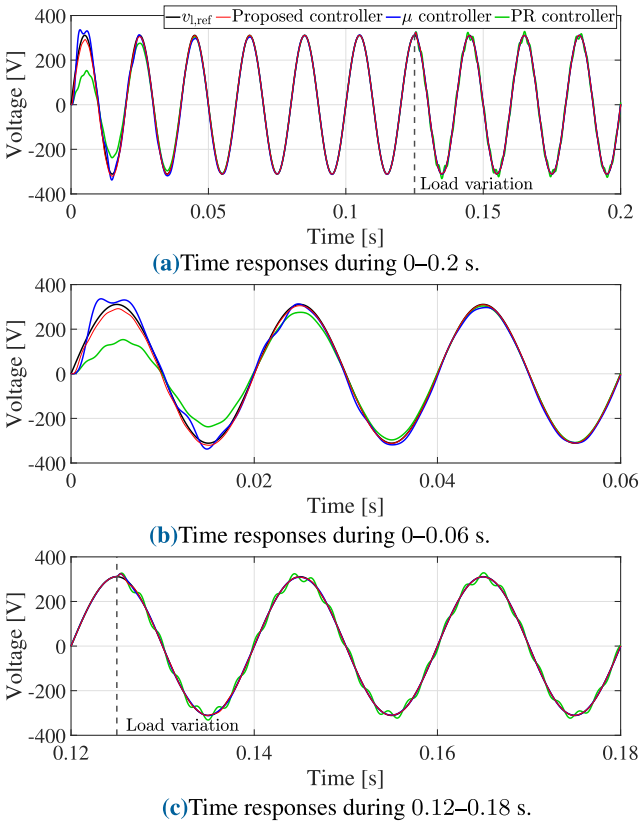

(a)Time responses during 0–0.2 s.

(b)Time responses during 0–0.06 s.

(c)Time responses during 0.12–0.18 s.

FIGURE 10. Voltage for linear load (simulation).

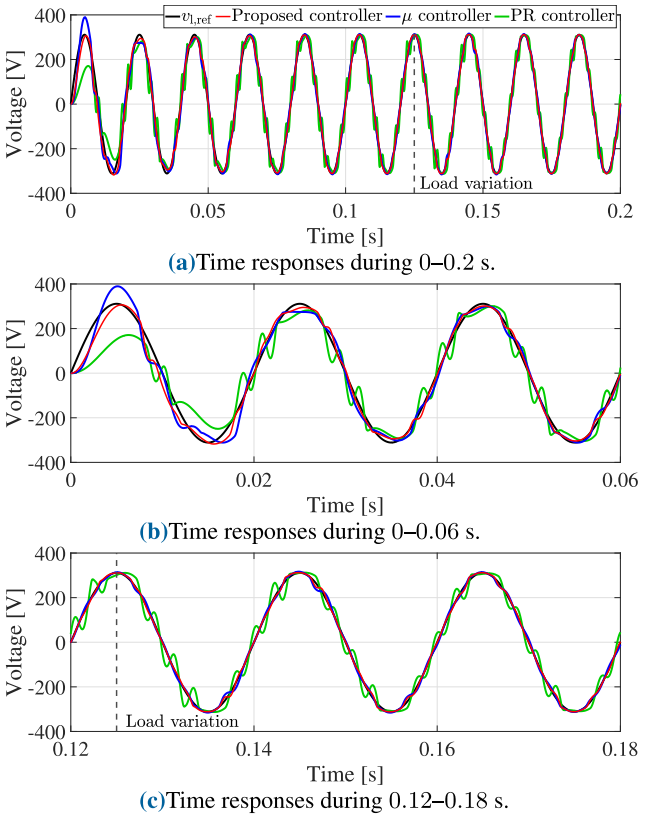

(a)Time responses during 0–0.2 s.

(b)Time responses during 0–0.06 s.

(c)Time responses during 0.12–0.18 s.

FIGURE 11. Voltage for nonlinear load (simulation).

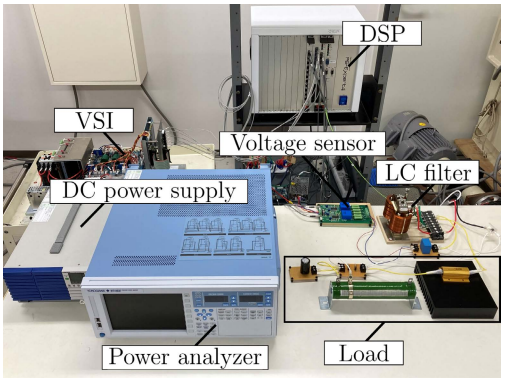

FIGURE 12. Experimental setup.

than the others, which implies v_l by the proposed controller converge to $v_{l,ref}$ faster than the others in both the linear and nonlinear loads. Moreover, the THD obtained with the proposed controller is sufficiently small.

Remark 1: The stability of the VSI with the nonlinear load with the μ-controller cannot be guaranteed theoretically. Specifically, the VSI with the μ-controller may be unstable depending on system parameters. By contrast, the controller obtained with the proposed design procedure guarantees robust stability of VSIs with not only linear but also nonlinear loads (See Appendix B for the stability analysis for nonlinear loads).

B. EXPERIMENTS

We show the experimental results. Fig. 12 shows the experimental setup. The control unit for the experiment is Myway Plus Corp. PE-Expert4 (DSP: TMS320C6657, 1.25 GHz).

In the experiment, the amplitude of $v_{l,ref}$ is changed from 0 to $\bar{v}_{l,n}$ at 0 s. Fig 13 shows the time responses of voltage for (a) linear and (b) nonlinear loads. It can be observed from Fig. 13 that the voltage responses by the proposed controller are faster than those by the others, as in the simulations. In addition, no overshoot or steady-state error appears in the voltage response by the proposed controller as in the simulations. Table 5 lists the $\mathcal{L}_{2e}$-norm ($\tau = 0.06$ s) and THD.[2] From Table 5, the $\mathcal{L}_{2e}$-norm and THD obtained with the proposed controller are sufficiently small, which implies that the proposed controller can achieve faster tracking and less distortion.

These simulation and experimental results validate that the proposed controller can stabilize VSIs for both linear

[2]THD is measured with the power analyzer (YOKOGAWA: WT1800E).

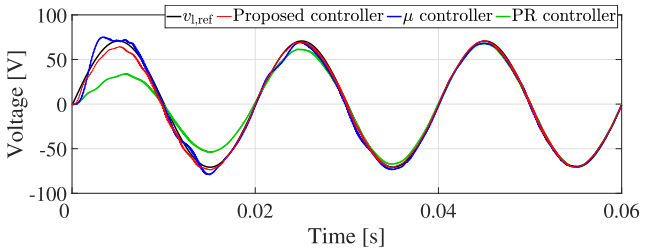

(a)Time responses for linear load.

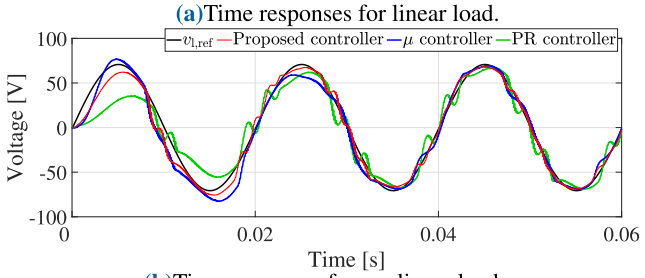

(b)Time responses for nonlinear load.

FIGURE 13. Voltage (experiment).

TABLE 5. Performance indices (experiment).

	Proposed	μ	PR
$\mathcal{L}_{2e}$-norm (linear load)	0.0156	0.0207	0.0632
$\mathcal{L}_{2e}$-norm (nonlinear load)	0.0352	0.0443	0.0742
THD (linear load) [%]	0.89	0.90	0.97
THD (nonlinear load) [%]	1.65	1.68	13.17

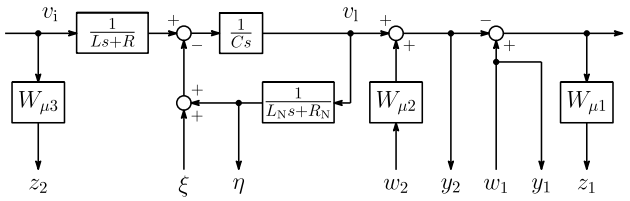

FIGURE 14. Generalized plant for μ-synthesis.

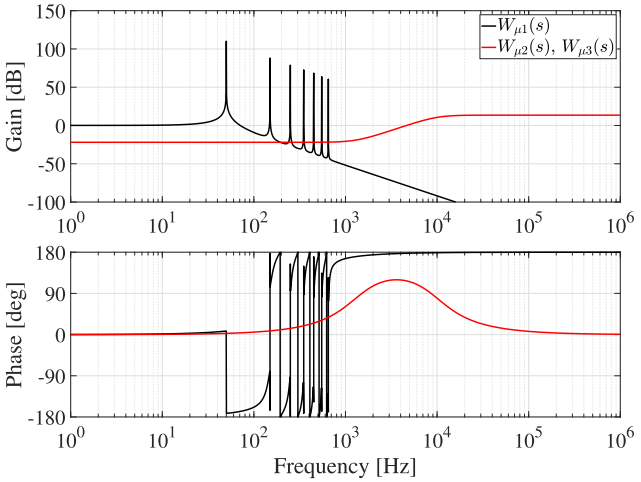

FIGURE 15. Weights in the μ-controller.

and nonlinear loads, achieving high-speed voltage responses. We therefore conclude that the proposed controller enables us to guarantee fast tracking, zero steady-state error, and low distortion in VSIs.

V. CONCLUSION

This paper proposed a novel voltage controller design procedure for VSIs. Comparative simulations and experiments clarified that the proposed controller could achieve fast tracking, zero steady-state error, and low distortion for sinusoidal voltage references in a VSI. The proposed controller also guarantees robust stability in VSIs with both linear and nonlinear loads. It should be noted that no information about unknown load is needed in advance, which is a remarkable contribution since no other design methodologies can solve such a complicated scenario.

We are presently extending the proposed design procedure to an integrated controller design for grid-connected inverters.

APPENDIX

A. DESIGN OF THE μ- AND PR CONTROLLERS

The μ-controller is based on μ-synthesis [23]. Figs. 14 and 15 show the generalized plant and the Bode plots of $W_{\mu j}(s)$ $(j = 1, 2, 3)$ for the μ-controller, respectively. In Fig. 14, $L_N = 1$ mH and $R_N = 1\ \Omega$. Fig. 16 shows the Bode plot of the μ-controller. The μ-controller has resonances at $i\omega_{ref}$ $(i = 1, 3, \ldots, 13)$, as with the proposed controller. However, the gain of the μ-controller in the high frequency domain is larger than that of the proposed controller since the μ-controller cannot be designed by $W_{\mu1}(s)$ and $W_{\mu2}(s)$ with a higher gain in the high frequency domain than those shown in Fig. 15.

The PR controller is tuned to achieve high performance in the nominal linear load listed in Table 3. It is given by

$$v_i^{ref} = \left(0.3 + \frac{200s}{s^2 + 1 \cdot 10^{-3}s + \omega_{ref}^2}\right)(v_l^{ref} - v_l). \quad (34)$$

B. STABILITY ANALYSIS FOR THE NONLINEAR LOAD

We analyze the stability of a VSI with a diode rectifier load (nonlinear load) in the proposed controller design procedure. Fig. 17 shows the equivalent circuit of Fig. 9. Fig. 18 shows the closed-loop system composed of the VSI with the controller designed by the proposed procedure and the diode rectifier load from terminal a-b shown in Fig. 17. Note that we treat the diode rectifier load from terminal a-b by $\Delta^\dagger$ as uncertainty.

First, we consider $-H_{\eta\xi}(s)$. Let the minimal state-space realization of $-H_{\eta\xi}$ be (A_1, B_1, C_1, D_1). We define the following Lyapunov function for $-H_{\eta\xi}(s)$:

$$V_1(x_1) = \frac{1}{2}x_1^\intercal P x_1, \quad (35)$$

where x_1 is the state of $-H_{\eta\xi}$ and $P > 0$ in a matrix, satisfying

$$\begin{bmatrix} A_1^\intercal P + PA_1 & PB_1 \\ B_1^\intercal P & 0 \end{bmatrix} - \begin{bmatrix} 0 & C_1^\intercal \\ C_1 & D_1 + D_1^\intercal \end{bmatrix} < 0. \quad (36)$$

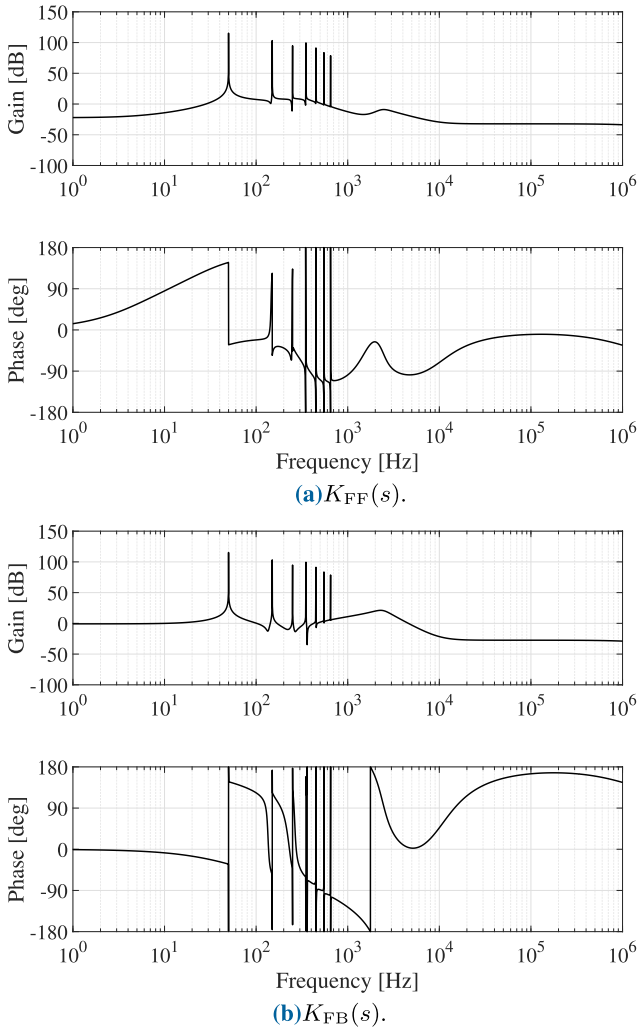

(a) $K_{\mathrm{FF}}(s)$.

(b) $K_{\mathrm{FB}}(s)$.

FIGURE 16. Bode plots of the μ-controller.

Since $-H_{\eta\xi}(s)$ is strongly positive-real, P exists in (36) [23].

Multiplying $\begin{bmatrix} x_1^{\mathsf{T}} & \eta^{\mathsf{T}} \end{bmatrix}^{\mathsf{T}} \neq 0$ and its transpose to (36) from right and left, respectively, we obtain

$$\dot{V}_1 < \xi\eta \tag{37}$$

with a simple calculation.

Second, we consider the diode rectifier load. From Fig. 17, we obtain the dynamics of the diode rectifier loads as follows:

$$C_{\mathrm{d}}\frac{\mathrm{d}v_{\mathrm{c}}}{\mathrm{d}t} + \frac{v_{\mathrm{c}}}{R_{\mathrm{d2}}} = |\eta|, \tag{38}$$

$$\mathrm{sgn}(-\eta)v_{\mathrm{c}} + (R_{\mathrm{s}} - R_{\mathrm{d1}})\eta = \xi, \tag{39}$$

$$-\eta = \begin{cases} \mathrm{sgn}(v_{\mathrm{l}})\dfrac{|v_{\mathrm{l}}| - |v_{\mathrm{c}}|}{R_{\mathrm{d1}}} & (|v_{\mathrm{l}}| - |v_{\mathrm{c}}| \geq 0), \\ 0 & (|v_{\mathrm{l}}| - |v_{\mathrm{c}}| < 0), \end{cases} \tag{40}$$

where $\mathrm{sgn}(\cdot)$ is the sign function defined by

$$\mathrm{sgn}(x) = \begin{cases} 1 & (x > 0), \\ 0 & (x = 0), \\ -1 & (x < 0). \end{cases} \tag{41}$$

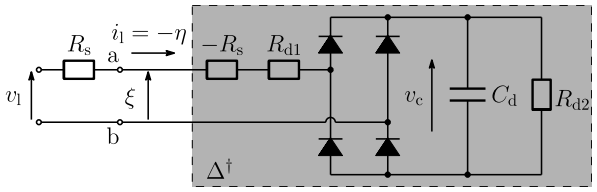

FIGURE 17. Equivalent circuit.

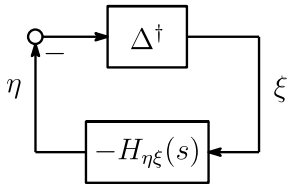

FIGURE 18. Closed-loop system of VSI with diode rectifier.

For (38), (39), and (40), we define

$$V_2(v_{\mathrm{c}}) = \frac{1}{2}C_{\mathrm{d}}v_{\mathrm{c}}^2. \tag{42}$$

From (38), (39) and (42), we obtain

$$\dot{V}_2(v_{\mathrm{c}}) = -\xi\eta + (R_{\mathrm{s}} - R_{\mathrm{d1}})\eta^2 - \frac{1}{R_{\mathrm{d2}}}v_{\mathrm{c}}^2. \tag{43}$$

Finally, we set $V(x_1, v_{\mathrm{c}}) = V_1(x_1) + V_2(v_{\mathrm{c}})$ as a Lyapunov function candidate of the closed-loop system shown in Fig. 18. It is clear that $V(x_1, v_{\mathrm{c}}) > 0$. From (37) and (43), we obtain

$$\dot{V}(x_1, v_{\mathrm{c}}) < (R_{\mathrm{s}} - R_{\mathrm{d1}})\eta^2 - \frac{1}{R_{\mathrm{d2}}}v_{\mathrm{c}}^2. \tag{44}$$

If $R_{\mathrm{s}} \leq R_{\mathrm{d1}}$ in (44), we obtain $\dot{V}(x_1, v_{\mathrm{c}}) < 0$. Therefore, the closed-loop system shown in Fig. 18 is asymptotically stable as long as $R_{\mathrm{s}} \leq R_{\mathrm{d1}}$.

REFERENCES

[1] K. P. Gokhale, A. Kawamura, and R. G. Hoft, "Dead beat microprocessor control of PWM inverter for sinusoidal output waveform synthesis," *IEEE Trans. Ind. Appl.*, vol. IA-23, no. 5, pp. 901–910, Sep. 1987.
[2] N. M. Abdel-Rahim and J. E. Quaicoe, "Analysis and design of a multiple feedback loop control strategy for single-phase voltage-source UPS inverters," *IEEE Trans. Power Electron.*, vol. 11, no. 4, pp. 532–541, Jul. 1996.
[3] Y. W. Li, "Control and resonance damping of voltage-source and current-source converters with *LC* filters," *IEEE Trans. Ind. Electron.*, vol. 56, no. 5, pp. 1511–1521, May 2009.
[4] F. M. Mahdianpoor, R. A. Hooshmand, and M. Ataei, "A new approach to multifunctional dynamic voltage restorer implementation for emergency control in distribution systems," *IEEE Trans. Power Del.*, vol. 26, no. 2, pp. 882–890, Apr. 2011.
[5] H. Komurcugil, "Rotating-sliding-line-based sliding-mode control for single-phase UPS inverters," *IEEE Trans. Ind. Electron.*, vol. 59, no. 10, pp. 3719–3726, Oct. 2012.
[6] L. Barote, C. Marinescu, and M. N. Cirstea, "Control structure for single-phase stand-alone wind-based energy sources," *IEEE Trans. Ind. Electron.*, vol. 60, no. 2, pp. 764–772, Feb. 2013.
[7] S. Mukherjee, P. Shamsi, and M. Ferdowsi, "Control of a single-phase standalone inverter without an output voltage sensor," *IEEE Trans. Power Electron.*, vol. 32, no. 7, pp. 5601–5612, Jul. 2017.
[8] S. S. Seyedalipour, M. Shahparasti, A. Hajizadeh, and M. Savaghebi, "Model-based control of four-leg inverter for UPS applications considering the effect of neutral line inductor," *IET Power Electron.*, vol. 14, no. 8, pp. 1468–1479, 2021.

[9] O. Kukrer, H. Komurcugil, and A. Doganalp, "A three-level hysteresis function approach to the sliding-mode control of single-phase UPS inverters," *IEEE Trans. Ind. Electron.*, vol. 56, no. 9, pp. 3477–3486, Sep. 2009.
[10] A. Abrishamifar, A. Ahmad, and M. Mohamadian, "Fixed switching frequency sliding mode control for single-phase unipolar inverters," *IEEE Trans. Power Electron.*, vol. 27, no. 5, pp. 2507–2514, May 2012.
[11] M. Monfared, S. Golestan, and J. M. Guerrero, "Analysis, design, and experimental verification of a synchronous reference frame voltage control for single-phase inverters," *IEEE Trans. Ind. Electron.*, vol. 61, no. 1, pp. 258–269, Jan. 2014.
[12] H. Komurcugil, N. Altin, S. Ozdemir, and I. Sefa, "An extended Lyapunov-function-based control strategy for single-phase UPS inverters," *IEEE Trans. Power Electron.*, vol. 30, no. 7, pp. 3976–3983, Jul. 2015.
[13] Z. Wang, Y. Yan, J. Yang, S. Li, and Q. Li, "Robust voltage regulation of a DC–AC inverter with load variations via a HDOBC approach," *IEEE Trans. Circuits Syst. II, Exp. Briefs*, vol. 66, no. 7, pp. 1172–1176, Jul. 2019.
[14] M. Parvez, M. F. M. Elias, N. A. Rahim, F. Blaabjerg, D. Abbott, and S. F. Al-Sarawi, "Comparative study of discrete PI and PR controls for single-phase UPS inverter," *IEEE Access*, vol. 8, pp. 45584–45595, 2020.
[15] Y. Peng, W. Sun, and F. Deng, "Internal model principle method to robust output voltage tracking control for single-phase UPS inverters with its SPWM implementation," *IEEE Trans. Energy Convers.*, vol. 36, no. 2, pp. 841–852, Jun. 2021.
[16] T.-S. Lee, S.-J. Chiang, and J.-M. Chang, "H_∞ loop-shaping controller designs for the single-phase ups inverters," *IEEE Trans. Power Electron.*, vol. 16, no. 4, pp. 473–481, Jul. 2001.
[17] G. Willmann, D. F. Coutinho, L. F. A. Pereira, and F. B. Libano, "Multiple-loop H_∞ control design for uninterruptible power supplies," *IEEE Trans. Ind. Electron.*, vol. 54, no. 3, pp. 1591–1602, Jun. 2007.
[18] S. Chakraborty, S. Patel, and M. V. Salapaka, "Robust and optimal single-loop voltage controller for grid-forming voltage source inverters," in *Proc. IEEE Power Energy Conf. Illinois (PECI)*, Feb. 2020, pp. 1–7.
[19] M. Ramezani, S. Li, and S. Golestan, "Analysis and controller design for stand-alone VSIs in synchronous reference frame," *IET Power Electron.*, vol. 10, no. 9, pp. 1003–1012, Jul. 2017.
[20] Y. Triki, A. Bechouche, H. Seddiki, and D. O. Abdeslam, "Improved D-Q frame controller for stand-alone single-phase inverters," in *Proc. IEEE Int. Conf. Ind. Technol. (ICIT)*, Feb. 2020, pp. 53–58.
[21] Y. Sato, T. Ishizuka, K. Nezu, and T. Kataoka, "A new control strategy for voltage-type PWM rectifiers to realize zero steady-state control error in input current," *IEEE Trans. Ind. Appl.*, vol. 34, no. 3, pp. 480–486, May/Jun. 1998.
[22] T. Kawabata, T. Miyashita, and Y. Yamamoto, "Dead beat control of three phase PWM inverter," *IEEE Trans. Power Electron.*, vol. 5, no. 1, pp. 21–28, Jan. 1990.
[23] K. Z. Liu and Y. Yao, *Robust Control Theory and Applications*. New York, NY, USA: Wiley, 2016.
[24] J. Teng, W. Gao, D. Czarkowski, and Z.-P. Jiang, "Optimal tracking with disturbance rejection of voltage source inverters," *IEEE Trans. Ind. Electron.*, vol. 67, no. 6, pp. 4957–4968, Jun. 2020.
[25] K.-Z. Liu, M. Ono, X. Li, and M. Wu, "Robust performance synthesis for systems with positive-real uncertainty and an extension to the negative-imaginary case," *Automatica*, vol. 82, pp. 194–201, Aug. 2017.
[26] H. K. Khalil, *Nonlinear Systems*, 3rd ed. Englewood Cliffs, NJ, USA: Prentice-Hall, 2002.
[27] A. Hasanzadeh, C. S. Edrington, B. Maghsoudlou, F. Fleming, and H. Mokhtari, "Multi-loop linear resonant voltage source inverter controller design for distorted loads using the linear quadratic regulator method," *IET Power Electron.*, vol. 5, no. 6, pp. 841–851, Jul. 2012.

KENTA KOIWA (Member, IEEE) was born in 1989. He received the B.E. and M.E. degrees in electrical engineering from the Kitami Institute of Technology, Japan, in 2012 and 2014, respectively, and the Ph.D. degree in electrical engineering from Chiba University, Japan, in 2017.

Since 2017, he has been an Assistant Professor with the Department of Electrical and Electronic Engineering, Chiba University. His research interests include power systems, renewable energy, and power electronics.

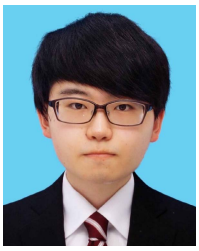

TAIKI GOTO received the B.E. degree in electrical engineering from Chiba University, Chiba, Japan, in 2022, where he is currently pursuing the M.E. degree. His research interest includes a robust controller design for voltage source inverter.

TADANAO ZANMA (Member, IEEE) was born in 1972. He received the B.S., M.S., and Dr.Eng. degrees from Nagoya University, in 1995, 1997, and 2000, respectively, all in electrical engineering.

From 2000 to 2007, he was a Research Associate at Mie University, where he has been an Assistant Professor, since 2007. In 2007, he was an Academic Guest with ETH Zurich. He was an Associate Professor at Mie University, from 2009 to 2011. He has been an Associate Professor with Chiba University, since 2011. His current research interests include hybrid dynamical control, switched systems, networked control systems, especially, system control based on mixed logical dynamical systems, and model predictive control.

He received the FANUC FA and Robot Foundation Thesis Prize, in 2009, and the IEEJ Distinguished Paper Award, in 2010 and 2015.

KANG-ZHI LIU (Senior Member, IEEE) received the B.E. degree in aeronautic engineering from Northwestern Polytechnical University, China, in 1984, and the M.E. and Ph.D. degrees in electrical engineering from Chiba University, Chiba, Japan, in 1988 and 1991, respectively.

He joined at Chiba University, where he is currently a Professor. He has authored six books. His main research interests include control theory, power systems, smart grids, and electrical drives.

He was the Director and the Executive Director of SICE, in 2017 and 2018, respectively. He was a recipient of the Young Author Award and the three Best Paper Awards from the Society of Instrument and Control Engineers (SICE), Japan.